# Algorithms for Multi-sensor and Multi-primitive Photogrammetric Triangulation

Sung Woong Shin, Ayman F. Habib, Mwafag Ghanma, Changjae Kim, and Eui-Myoung Kim

**The steady evolution of mapping technology is leading to an increasing availability of multi-sensory geo-spatial datasets, such as data acquired by single-head frame cameras, multi-head frame cameras, line cameras, and light detection and ranging systems, at a reasonable cost. The complementary nature of the data collected by these systems makes their integration to obtain a complete description of the object space. However, such integration is only possible after accurate co-registration of the collected data to a common reference frame. The registration can be carried out reliably through a triangulation procedure which considers the characteristics of the involved data. This paper introduces algorithms for a multi-primitive and multi-sensory triangulation environment, which is geared towards taking advantage of the complementary characteristics of spatial data available from the above mentioned sensors. The triangulation procedure ensures the alignment of involved data to a common reference frame. The devised methodologies are tested and proven efficient through experiments using real multi-sensory data.**

**Keywords: Frame camera, line camera, LIDAR, linear primitives, areal primitives, multi-sensor triangulation.**

Manuscript received Oct. 10, 2006; revised June 26, 2007.

This work was partly supported by the IT R&D program of MIC/IITA [2007-F-042-01, Technology Development for 3D GIS-Based Wave Propagation Analysis], the GEOIDE (SII #43) (GEOmatics for Informed DEcisions) Networks of Centers of Excellence, and NSERC (Natural Sciences and Engineering Research Council of Canada).

Sung Woong Shin (phone: + 82 42 869 1783, email: sshin@etri.re.kr) is with Telematics & USN Research Division, ETRI, Daejeon, S. Korea.

Ayman F. Habib (email: habib@geomatics.ucalgary.ca) and Changjae Kim (email: cjkim@ucalgary.ca) are with the Department of Geomatics Engineering, University of Calgary, Alberta, Canada.

Mwafag Ghanma (email: msghanma@ucalgary.ca) is with the Department of Surveying and Geomatics Engineering, Al-Balqa' Applied University, Al-Salt, Jordan.

Eui-Myoung Kim (email: kemyoung@nsu.ac.kr) is with the Department of GIS Engineering, Namseoul University, Cheonan, S. Korea.

## I. Introduction

A diverse range of spatial data acquisition systems is now available onboard satellite, aerial, and terrestrial mapping platforms. The diversity includes analog and digital frame cameras and linear array scanners. In the past few years, imaging sensors witnessed vast development as a result of rapid advancement in digital technology. For example, the increasing sensor size and storage capacity of digital frame cameras has led to their application in new and traditional mapping functions. However, due to technical limitations, single-head frame cameras are not capable of providing geometric resolution and ground coverage similar to those associated with analog frame cameras. To alleviate this limitation, multi-head frame cameras and push-broom scanners (line cameras) have been developed and used onboard satellite and aerial platforms. In addition to imaging systems, light detection and ranging (LIDAR) scanning is rapidly taking its place in the mapping industry as a fast and cost-effective 3D data acquisition technology.

Considering the characteristics of spatial data acquired from imaging and LIDAR systems, one can argue that their integration will be beneficial for accurate and complete description of the object space. As an illustration of the complementary characteristics of imaging and LIDAR systems, Tables 1 and 2 list the advantages and disadvantages of each system in relation to the disadvantages and the advantages of the other system. As these tables demonstrate, the disadvantages of one system can be compensated for by the advantages of the other system [1], [2]. However, the synergic characteristics of both systems can be fully utilized only after ensuring that both datasets are geo-referenced relative to the same reference frame [3], [4].

Table 1. Photogrammetric strengths in relation to LIDAR weaknesses.

| Photogrammetric Pros | LIDAR Cons |
|---|---|
| High redundancy | No inherent redundancy |
| Rich in semantic information | Positional; difficult to derive semantic information |
| Dense positional information along object space break lines | Almost no information along break lines |
| Planimetric accuracy is better than the vertical accuracy | Planimetric accuracy is worse than the vertical accuracy |

Table 2. LIDAR strengths in relation to photogrammetric weaknesses.

| LIDAR Pros | Photogrammetric Cons |
|---|---|
| Dense information along homogeneous surfaces | Almost no positional information along homogeneous surfaces |
| Day or night data collection | Day time data collection |
| Direct acquisition of 3D coordinates | Complicated and sometimes unreliable matching procedures |
| Vertical accuracy is better than the planimetric accuracy | Vertical accuracy is worse than the planimetric accuracy |

Traditionally, photogrammetric geo-referencing has been either indirectly established with the help of ground control points (GCP) or directly defined using GPS/INS units on board the imaging platform [5], [6]. On the other hand, LIDAR geo-referencing is directly established through the GPS/INS components of a LIDAR system. This paper presents alternative methods for utilizing LIDAR features as a source of control for photogrammetric geo-referencing. These methods have two main advantages. First, they ensure the co-alignment of the LIDAR and photogrammetric data to a common reference frame as defined by the GPS/INS unit of the LIDAR system. Moreover, LIDAR features eliminate the need for ground control points to establish the geo-referencing parameters of the photogrammetric data. The possibility of utilizing LIDAR data as a source of control for photogrammetric geo-referencing hinges on the ability to identify common features in both datasets. Therefore, the first objective of the developed methods is the selection of appropriate primitives. Afterwards, the mathematical models, which can be utilized in the triangulation procedure for establishing the relationship between LIDAR and photogrammetric primitives, are introduced. Another objective for the proposed methods is to make them flexible enough to allow for the incorporation of the identified primitives in the scenes captured by frame and line cameras. In other words, the developed methods should handle multi-sensory data while using a wide range of primitives (as in multi-primitive and multi-sensor triangulation methods).

The remainder of this paper is organized as follows. Sections II and III offer a brief discussion of LIDAR and photogrammetric principles. The discussion of the photogrammetric principles focuses on the possibility of incorporating frame and line cameras into a single triangulation mechanism. Sections IV and V address the primitive selection to relate the LIDAR and photogrammetric data as well as the respective mathematical models for their incorporation into the triangulation procedure. In section VI, the feasibility and the performance of the developed multi-primitive and multi-sensor triangulation procedure are established through experimental results using real data. Finally, in section VII, the paper concludes with final remarks and recommendations for future research.

## II. LIDAR Principles

The LIDAR system has been conceived to directly and accurately capture digital surfaces. The affordability, improved direct geo-referencing capabilities, increased pulse frequency, and versatility of the new LIDAR systems are causing an exponential profusion of these systems in the mapping industry. A LIDAR system comprises two main units: laser ranging and GPS/INS systems (see Fig. 1). Positional information derived from LIDAR systems is based on calculating the range between the laser unit and the object space. As shown in Fig. 1, the measured range is coupled with the position and orientation information, as determined by the onboard GPS/INS unit, to directly determine the position of the laser footprint through a vector summation procedure.

In addition to the derived positional information, the intensity of the signal echo is also recorded by recent LIDAR scanners (see Fig. 2). The visualization of the intensity map can be used for object space segmentation and feature extraction. However, it is still difficult to derive semantic information regarding the

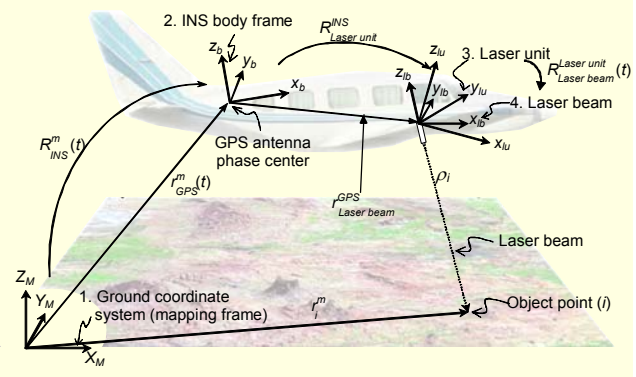


Fig. 1. Coordinate systems and parameters involved in direct geo-referencing of LIDAR systems.


Fig. 2. Visualization of LIDAR coverage: (a) shaded-relief map of range data and (b) intensity image.

captured surfaces (such as material and types of observed structures) using the intensity image [1], [7], [8].

## III. Photogrammetric Principles

Since photogrammetric operations using frame cameras are well established, the focus of this section is on the utilization of line cameras in photogrammetric triangulation. We also investigate the possibility of incorporating frame and line cameras in a single triangulation mechanism. As previously mentioned, the majority of imaging satellites implement a line camera which has a single linear array in the focal plane. This is in contrast to the two-dimensional array of a frame camera (see Fig. 3). A single exposure of this linear array covers a narrow strip in the object space. Continuous coverage of contiguous areas on the ground is achieved by moving the imaging platform while leaving the shutter open. In this regard, a distinction is made between a scene and an image. An image is obtained through a single exposure of the light sensitive elements in the focal plane, whereas a scene covers a two-dimensional area in the object space and might be composed of one or multiple images depending on the nature of the camera implemented. According to this distinction, a scene captured by a frame camera consists of a single image, whereas a scene captured by a line camera is composed of multiple images.

For frame and line cameras, the collinearity equations mathematically state that the perspective center, the image point, and the corresponding object point are aligned along a straight line. For a line camera, the collinearity model can be

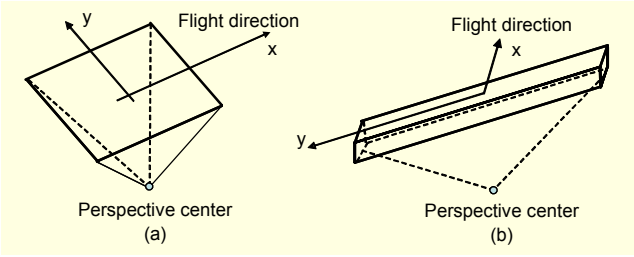


Fig. 3. Imaging sensors: (a) frame camera and (b) line camera.

described by (1). It should be noted that the collinearity equations involve the image coordinates ($x_i$, $y_i$), which are equivalent to the scene coordinates ($x_s$, $y_s$), when dealing with a scene captured by a frame camera. For line cameras, however, the scene coordinates ($x_s$, $y_s$) need to be transformed into image coordinates. In this case, the $x_s$ value is used to indicate the moment of exposure of the corresponding image. On the other hand, the $y_s$ value is directly related to the $y_i$ image coordinate (see Fig. 4). It should be noted that the $x_i$ image-coordinate in (1) is a constant which depends on the alignment of the linear array in the focal plane:

$$x_i = x_p - c\frac{r_{11}^t(X_G - X_O^t) + r_{21}^t(Y_G - Y_O^t) + r_{31}^t(Z_G - Z_O^t)}{r_{13}^t(X_G - X_O^t) + r_{23}^t(Y_G - Y_O^t) + r_{33}^t(Z_G - Z_O^t)},$$

$$y_i = y_p - c\frac{r_{12}^t(X_G - X_O^t) + r_{22}^t(Y_G - Y_O^t) + r_{32}^t(Z_G - Z_O^t)}{r_{13}^t(X_G - X_O^t) + r_{23}^t(Y_G - Y_O^t) + r_{33}^t(Z_G - Z_O^t)}, \quad (1)$$

where ($X_G$, $Y_G$, $Z_G$) are the ground coordinates of the object point; $(X_O^t, Y_O^t, Z_O^t)$ are the ground coordinates of the perspective center at the moment of exposure, $r_{11}^t$ through $r_{33}^t$ are the elements of the rotation matrix at the moment of exposure, ($x_i$, $y_i$) are the image coordinates of the point under consideration, and ($x_p$, $y_p$, $c$) are the interior orientation parameters (IOPs) of the imaging sensor.

Another difference between the collinearity equations for frame and line cameras is the multiple exposures associated with a line camera scene in contrast to the single exposure for an image captured by a frame camera. Therefore, the exterior orientation parameters (EOPs) associated with a line camera scene are time dependent and vary depending on the image considered within the scene. For practical reasons, the bundle adjustment of scenes captured by line cameras does not consider all the involved exterior orientation parameters. It would lead to an excessive number of parameters requiring an extensive amount of control. To avoid such a problem, the bundle adjustment of scenes captured by line cameras

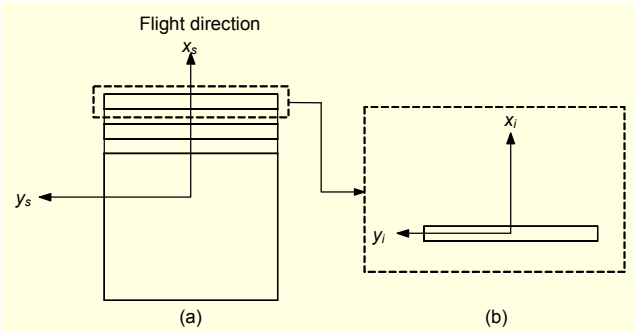


Fig. 4. (a) Scene coordinate system and (b) image coordinate system for a line camera.

implements one of two reduction approaches [9]. In the first approach, the system's trajectory and attitude are assumed to follow a polynomial trend with time as the independent variable. Therefore, the unknown exterior orientation parameters are reduced to the number of coefficients involved in the assumed polynomials. Available knowledge regarding the trajectory of the imaging system can be used as prior information regarding the polynomial coefficients, leading to what is known as the physical sensor model [10]. Another approach to reduce the number of the involved exterior orientation parameters is based on the principal of orientation images which are equally spaced along the system's trajectory. The exterior orientation parameters at any given time are modeled as a weighted average of the exterior orientation parameters associated with the neighboring orientation images. In this way, the number of exterior orientation parameters for a given scene is reduced to the number of parameters associated with the orientation images involved.

It should be noted that the imaging geometry associated with line cameras (including the reduction methodology of the involved EOP) is more general than that of frame cameras. In other words, the imaging geometry of a frame camera can be derived as a special case of that for a line camera. For example, an image captured by a frame camera can be considered a special case of a scene captured by a line camera in which the trajectory and attitude are represented by a zero-order polynomial. Alternatively, when working with orientation images, a frame image can be considered a line camera scene with one orientation image. The general nature of the imaging geometry of line cameras lends itself to straightforward development of multi-sensor triangulation procedures capable of incorporating frame and line cameras [11], [12].

Having discussed LIDAR and photogrammetric principles, in the next section we deal with the selection, representation, and extraction of appropriate primitives from LIDAR and photogrammetric data. This discussion is followed by the derivation of the necessary mathematical models to incorporate these primitives into the photogrammetric triangulation.

## IV. Triangulation Primitives

A triangulation process relies on the identification of common primitives to relate the datasets involved to the reference frame defined by the control information. Traditionally, photogrammetric triangulation has been based on point primitives. However, LIDAR data consists of discontinuous and irregular footprints, in contrast to photogrammetric data, which is acquired from continuous and regular scanning of the object space. Considering the characteristics of photogrammetric and LIDAR data, relating a LIDAR footprint to the corresponding point in imagery is almost impossible (see Fig. 5).

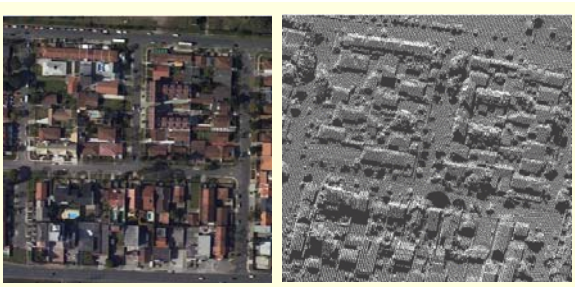

Fig. 5. (a) Imagery and (b) LIDAR coverage of an urban area.

Three intersecting patches can be segmented from LIDAR range data and utilized to extract accurate points at a higher processing cost. Therefore, point primitives are not appropriate for the task at hand. Linear and areal features are other potential primitives that can be more suitable for relating LIDAR and photogrammetric data. Linear features can be directly identified in imagery, while conjugate LIDAR lines can be extracted through planar patch segmentation and intersection. Alternatively, LIDAR lines can be directly identified in the intensity images produced by most of today's LIDAR systems.

It should be noted that linear features extracted from planar patch segmentation and intersection are more accurate than the features extracted from intensity images. The lower quality of the features extracted from the intensity images is caused by the utilized interpolation procedure to convert the irregular LIDAR footprints to a raster grid. Other than linear features, areal primitives in photogrammetric datasets can be defined using their boundaries, which can be identified in the imagery. Such primitives include, for example, rooftops, lakes, and other homogeneous regions. In LIDAR datasets, areal regions can be derived through planar patch segmentation techniques.

Another issue related to primitive selection is their representation in both photogrammetric and LIDAR data. In this regard, image space lines can be represented by a sequence of image points along the feature (see Fig. 6(a)). This is an appealing representation since it can handle image space linear features in the presence of distortions which cause deviations from straightness in the image space. Moreover, such a representation allows the inclusion of linear features in scenes captured by line cameras, since perturbations in the flight trajectory lead to deviations from straightness in the image space linear features corresponding to object space straight lines. It should be noted that the selected intermediate points along corresponding line segments in overlapping scenes need not be conjugate. As for the LIDAR data, object lines can be represented by their end points (see Fig. 6(b)).

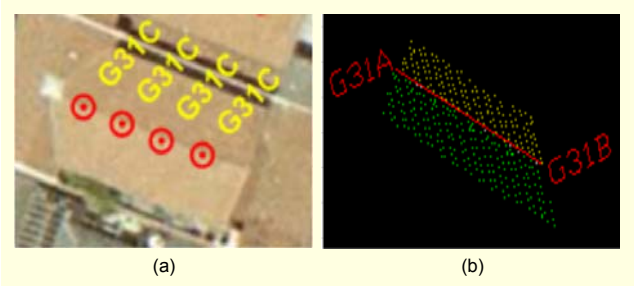


(a) (b)

Fig. 6. (a) Image space linear features defined by a sequence of intermediate points and (b) corresponding LIDAR lines defined by their end points.

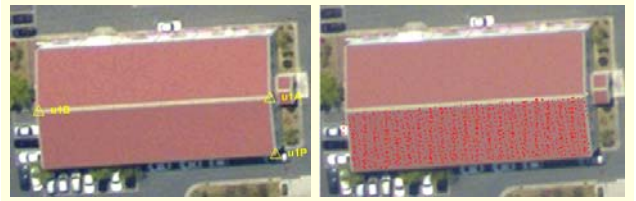

(a) (b)

Fig. 7. (a) Image space planar features represented by three points and (b) LIDAR patches defined by the points comprising the patch.

The points defining the LIDAR line need not be visible in the imagery.

When using areal primitives, photogrammetric planar patches can be represented by three points, namely, corner points, as shown in Fig. 7(a), along their boundaries. These points should be identified in all overlapping imagery. Like linear features, this representation is valid for scenes captured by frame and line cameras. On the other hand, LIDAR patches can be represented by the footprints defining that patch (see Fig. 7(b)). These points can be derived directly using planar patch segmentation techniques.

## V. Mathematical Models

### 1. Utilizing Straight Linear Primitives

This subsection focuses on deriving the mathematical constraint for relating LIDAR and photogrammetric lines, which are represented by the end points in the object space and a sequence of intermediate points in the image space, respectively. From this perspective, the photogrammetric datasets will be aligned to the LIDAR reference frame through direct incorporation of LIDAR lines as the source of control.

The photogrammetric and LIDAR measurements along corresponding linear features can be related to each other through the coplanarity constraint in (2). This constraint indicates that the vector from the perspective center to any intermediate image point along the image line is contained within the plane defined by the perspective center of that image and the two points defining the LIDAR line. In other words, for a given intermediate point, $k''$, the points $\{(\mathbf{X_1}, \mathbf{Y_1}, \mathbf{Z_1}), (\mathbf{X_2}, \mathbf{Y_2}, \mathbf{Z_2}), (\mathbf{X''_O}, \mathbf{Y''_O}, \mathbf{Z''_O})$, and $(\mathbf{x_{k''}}, \mathbf{y_{k''}}, \mathbf{0})\}$ are coplanar (see Fig. 8).

$$(\vec{\mathbf{V}}_1 \times \vec{\mathbf{V}}_2) \cdot \vec{\mathbf{V}}_3 = 0, \tag{2}$$

where $\vec{\mathbf{V}}_1$ is the vector connecting the perspective center to the first end point along the LIDAR line, $\vec{\mathbf{V}}_2$ is the vector connecting the perspective center to the second end point along the LIDAR line, and $\vec{\mathbf{V}}_3$ is the vector connecting the perspective center to an intermediate point along the corresponding image line.

It should be noted that the above constraint can be introduced for all intermediate points along the image space linear feature. Moreover, the coplanarity constraint is valid for both frame and line cameras. For scenes captured by line cameras, the involved EOPs should correspond to the image associated with the intermediate point under consideration. For frame cameras with known IOPs, a maximum of two independent constraints can be defined for a given image. However, in self-calibration procedures, additional constraints help in the recovery of the IOPs since the distortion pattern will change from one intermediate point to the next along the image space linear feature. On the other hand, the coplanarity constraint helps in better recovery of the EOPs associated with line cameras. Such a contribution is attributed to the fact that the system's trajectory will affect the shape of the linear feature in the image space.

For an image block, at least two non-coplanar line segments are needed to establish the datum of the reconstructed object space, namely, the scale, rotation, and shift components. Such a requirement assumes that a model can be derived from the image block and is explained by the fact that a single line defines

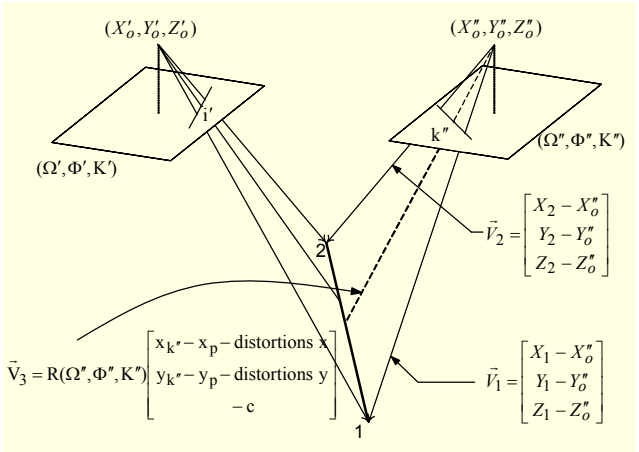


Fig. 8. Perspective transformation between image and LIDAR straight lines and the coplanarity constraint for intermediate points along the line.

two shift components across the line as well as two rotation angles (as defined by the line heading and pitch). Having another non-coplanar line helps in estimating the remaining shift and rotation components as well as the scale factor.

### 2. Utilizing Planar Patches

This subsection focuses on deriving the mathematical constraint for relating LIDAR and photogrammetric patches, which are represented by a set of points in the object space and three points in the image space, respectively. As an example, let us consider a surface patch which is represented by two sets of points, namely, the photogrammetric set $S_{PH}$= {A, B, C} and the LIDAR set $S_L$= {($X_P$, $Y_P$, $Z_P$), P=1 to n} (see Fig. 9). Since the LIDAR points are randomly distributed, no point-to-point correspondence can be assumed between the datasets. For the photogrammetric points, the image and object space coordinates are related to each other through the collinearity equations. On the other hand, LIDAR points belonging to a certain planar-surface patch should coincide with the photogrammetric patch representing the same object space surface (see Fig. 9). The coplanarity of the LIDAR and photogrammetric points can be mathematically expressed as

$$V = \begin{vmatrix} X_P & Y_P & Z_P & 1 \\ X_A & Y_A & Z_A & 1 \\ X_B & Y_B & Z_B & 1 \\ X_C & Y_C & Z_C & 1 \end{vmatrix} = \begin{vmatrix} X_P - X_A & Y_P - Y_A & Z_P - Z_A \\ X_B - X_A & Y_B - Y_A & Z_B - Z_A \\ X_C - X_A & Y_C - Y_A & Z_C - Z_A \end{vmatrix} = 0. \quad (3)$$

The above constraint is used as the mathematical model for incorporating LIDAR points into the photogrammetric triangulation. In physical terms, this constraint means that the normal distance between any LIDAR point and the corresponding photogrammetric surface should be zero, or the volume of the tetrahedron composed of the four points is equal to zero. This constraint is applied to all LIDAR points comprising this surface patch. It should be noted that the above constraint is valid for both frame and line cameras.

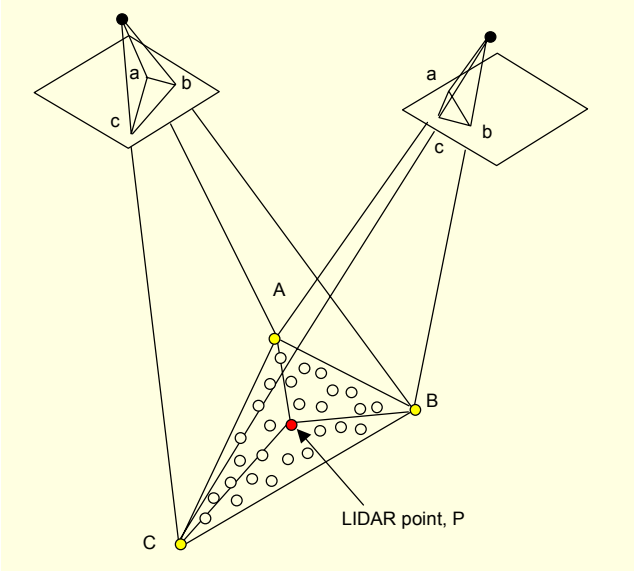

Fig. 9. Coplanarity of photogrammetric and LIDAR patches.

To be sufficient as the only source of control, LIDAR patches should be able to provide all the data parameters, three translations ($X_T$, $Y_T$, $Z_T$), three rotations (ω, ϕ, κ), and one scale factor (S). Figure 10 demonstrates that a patch normal to one of the axes will provide the shift in the direction of that axis as well as the rotation angles across the other axes. Therefore, three non-parallel patches are sufficient to determine the position and orientation components of the datum. For scale determination, the three planar patches should not intersect at a single point (as for example, facets of a pyramid). Alternatively, the scale can be determined by incorporating a fourth plane, as shown in Fig. 10. However, the probability of having vertical patches in airborne LIDAR data is not high. Therefore, instead of working with vertical patches, one can use tilted patches with varying slopes and aspects.

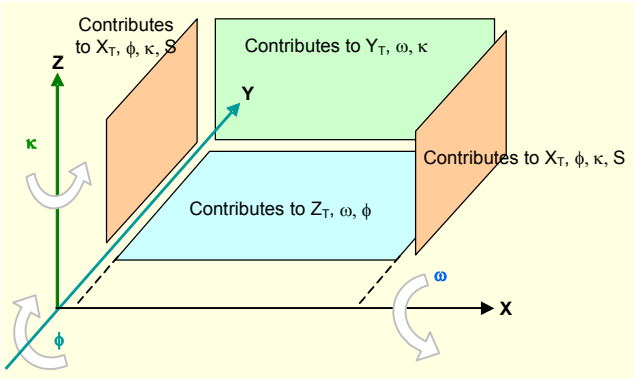

Fig. 10. Optimal configuration for establishing the datum using planar patches as the source of control.

## VI. Experimental Results

To validate the feasibility and applicability of the above methods, multi-sensory datasets were solicited and analyzed. The conducted experiments involved four types of sensors, namely, a digital frame camera equipped with a GPS receiver, a satellite-based line camera, and a LIDAR system. These experiments investigated the following issues:

- the validity of using the line-based geo-referencing procedure for scenes captured by frame and line cameras
- the validity of using the patch-based geo-referencing procedure for scenes captured by frame and line cameras

- the impact of integrating satellite scenes, aerial scenes, LIDAR data, and GPS positions of the exposures in a unified bundle adjustment procedure

The first dataset comprises three blocks of 6-frame digital images captured in April 2005, by the Applanix Digital Sensor System (DSS) over the city of Daejeon in South Korea, from an altitude of 1500 m. The DSS camera had 16 mega pixels (9 μm pixel size) and a 55 mm focal length. The position of the DSS camera was tracked using an onboard GPS receiver. The second dataset consisted of an IKONOS stereo-pair, which was captured in November 2001, over the same area. It should be noted that these scenes were raw imagery that did not go through any geometric correction and were provided for research purposes. Finally, a multi-strip LIDAR coverage, corresponding to the DSS coverage, was collected using the OPTECH ALTM 3070 with an average point density of 2.67 point/$m^2$, from an altitude of 975 m. An example of one of the DSS image blocks and a visualization of the corresponding LIDAR coverage is shown in Fig. 11. Figure 12 shows the IKONOS coverage and the location of the DSS image blocks.

To extract the LIDAR control, a total of 139 planar patches with different slopes and aspects and 138 linear features were manually identified through planar patch segmentation and intersection, respectively. Figure 11 shows the locations of the

(a)

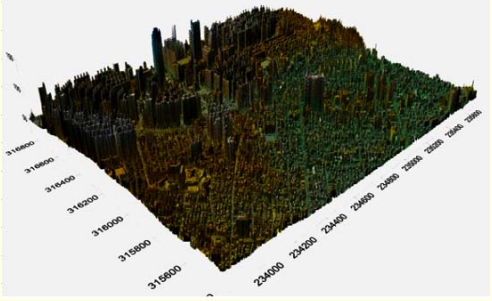

(b)

Fig. 11. (a) DDS middle image block and (b) the corresponding LIDAR cloud. The circles in (a) indicate the location of linear and areal primitives extracted from the LIDAR data.

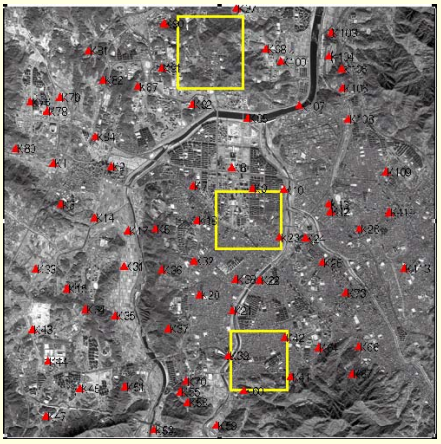

Fig. 12. IKONOS scene coverage with the three patches covered by the DSS imagery and LIDAR data.

features extracted from the middle LIDAR point cloud within the IKONOS scenes. The corresponding linear and areal features were digitized in the DSS and IKONOS scenes. To evaluate the performance of the different geo-referencing techniques, a set of 70 ground control points (GCP) was also acquired. The distribution of these points is shown in Fig. 12. The performance of the point-based, line-based, patch-based, and GPS-assisted geo-referencing techniques was assessed using root mean square error (RMSE) analysis. In the different experiments, a portion of the available GCP was used as control in the bundle adjustment, while the rest were used as check points. None of the available control points are visible in any of the DSS imagery.

To investigate the performance of the various geo-referencing methods, we conducted the following experiments:

- photogrammetric triangulation of the IKONOS scenes while varying the number of utilized GCPs
- photogrammetric triangulation of the IKONOS and DSS scenes while varying the number of utilized GCPs
- photogrammetric triangulation of the IKONOS and DSS scenes while considering the GPS observations associated with the DSS exposures and varying the number of utilized GCPs
- photogrammetric triangulation of the IKONOS and DSS scenes while varying the number of LIDAR lines (45 and 138 lines) together with changing the number of GCPs
- photogrammetric triangulation of the IKONOS and DSS scenes while varying the number of LIDAR patches (45 and 139 patches) together with changing the number of GCPs

The resulting total RMSE values for these experiments are reported in Table 3.

In Table 3, the "N/A" means that no solution was attainable.

That is, the provided control was not sufficient to establish the datum for the triangulation procedure. For more clarity, the results in Table 3 are aggregated visually in Fig. 13, in which the total RMSE values are plotted against the number of control points for the different geo-referencing techniques. Table 3 and Fig. 13 demonstrate the following:

- Utilizing points as the only source of control for the triangulation of the stereo IKONOS scenes requires a minimum of six GCPs.
- Including DSS imagery with the IKONOS scenes in the triangulation reduced the control requirement for convergence to three GCPs. Moreover, the incorporation of the GPS observations at the DSS exposure stations enabled convergence without the need for any ground control points. Therefore, it is clear that incorporating satellite scenes with a few frame images would allow photogrammetric reconstruction while reducing the ground control point requirements.
- LIDAR linear features are sufficient for geo-referencing the IKONOS and DSS scenes without the need for any additional sources of control. As the fifth and sixth columns of Table 3 show, incorporating additional control points in the triangulation procedure does not significantly improve the reconstruction outcome. Moreover, by comparing the fifth and sixth columns, one can see that increasing the linear features from 45 to 138 does not significantly improve the quality of the triangulation outcome.

LIDAR patches are sufficient for geo-referencing the IKONOS and DSS scenes without the need for an additional source of control. However, the seventh and eighth columns of Table 3 show that incorporating a few control points significantly improved the results (using 3 GCPs and 139 control patches, the total RMSE was reduced from 5.4 m to 2.9 m). Incorporating additional control points (beyond 3 GCPs) did not have a significant impact. The improvement in the reconstruction outcome as a result of using a few GCPs can be attributed to the fact that the majority of the utilized patches were horizontal with mild slopes, as they represented building roofs. Therefore, the estimation of the model shifts in the X and Y directions was not accurate enough. Incorporating vertical or steep patches could have solved this problem. However, such patches were not available in the provided dataset. Moreover, comparison of the seventh and eighths columns shows that increasing the number of control patches from 45 to 139 did not significantly improve the quality of the triangulation outcome.

Comparing the different geo-referencing techniques demonstrates that the patch-based, line-based, and GPS-assisted geo-referencing techniques resulted in better outcomes than point-based geo-referencing. Such an improvement demonstrates the benefit of adopting multi-sensor and multi-primitive triangulation procedures.

In an additional experiment, we utilized the EOP derived from the multi-sensor triangulation of the frame and line camera scenes together with the LIDAR surface to generate orthophotos. Figure 14 shows sample patches, in which the IKONOS and DSS orthophotos are laid side by side. As seen in Fig. 14(a), the generated orthophotos are quite compatible, as demonstrated by the smooth continuity of the observed features between the DSS and IKONOS orthophotos. Figure 14(b) shows object space changes between the moments of

Table 3. Check-point analysis for multi-sensor and multi-primitive triangulation.

| # of GCPs | IKONOS only | IKONOS + 18 DSS frame images | | | | | |
|---|---|---|---|---|---|---|---|
| | Control points only | Control points only | Control points plus | | | | |
| | | | DSS GPS | Control lines | | Control patches | |
| | | | | 138 | 45 | 139 | 45 |
| 0 | N/A | N/A | 3.1 | 3.1 | 3.1 | 5.4 | 5.9 |
| 1 | N/A | N/A | 3.4 | 3.0 | 3.1 | 5.4 | 6.4 |
| 2 | N/A | N/A | 3.1 | 3.1 | 3.2 | 4.8 | 5.2 |
| 3 | N/A | 21.3 | 2.9 | 2.9 | 2.8 | 2.9 | 3.1 |
| 4 | N/A | 20.0 | 2.8 | 2.7 | 2.8 | 2.6 | 3.1 |
| 5 | N/A | 4.3 | 2.7 | 2.7 | 2.7 | 2.6 | 2.7 |
| 6 | 3.7 | 3.4 | 2.7 | 2.7 | 2.7 | 2.6 | 2.7 |
| 7 | 3.9 | 3.0 | 26 | 2.7 | 2.7 | 2.5 | 2.6 |
| 8 | 3.6 | 3.4 | 2.6 | 2.6 | 2.5 | 2.5 | 2.7 |
| 9 | 4.1 | 2.5 | 2.5 | 2.6 | 2.5 | 2.4 | 2.5 |
| 10 | 3.1 | 2.5 | 2.5 | 2.6 | 2.5 | 2.4 | 2.5 |
| 15 | 3.2 | 2.4 | 2.5 | 2.5 | 2.4 | 2.4 | 2.4 |
| 40 | 2.0 | 2.1 | 2.1 | 2.1 | 2.1 | 2.0 | 2.0 |

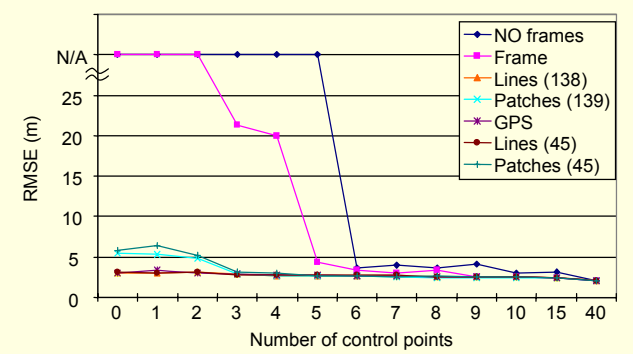


Fig. 13. Check point analysis from the bundle adjustments involving IKONOS and DSS imagery as well as LIDAR features for various control configurations.

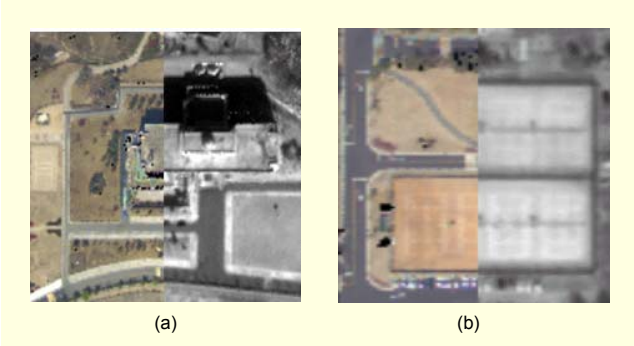


Fig. 14. Change detection between DSS (color) and IKONOS (B/W) orthophotos. Smooth transition between the two orthophotos can be observed in (a), while discontinuities are observed in (b) due to changes in the object space.

capture of the IKONOS and DSS imagery. Therefore, it is evident that multi-sensor triangulation of imagery from frame and line cameras improves the quality of the derived object space while offering an environment for accurate geo-referencing of the temporal imagery. Following geo-referencing, the involved imagery can be analyzed for change detection applications using the derived and properly geo-referenced orthophotos.

## VII. Conclusion and Recommendations for Future Work

The continuing advancements in mapping technology demand the development of commensurate processing methods to take advantage of the synergistic characteristics of available geo-spatial data. In this regard, it is quite evident that integrating LIDAR and photogrammetric data is essential for ensuring an accurate and complete description of the object space. This paper presented methods for aligning LIDAR and photogrammetric data relative to a common reference frame using linear and areal primitives. The developed methods are suited to the characteristics of these datasets. Moreover, the introduced methods are general enough, in the sense they can be applied directly to scenes captured by line and frame cameras. The experimental results demonstrated that the utilization of LIDAR derived primitives as the source of control for photogrammetric geo-referencing yields slightly better results when compared with point-based geo-referencing techniques. Moreover, it was shown that the incorporation of sparse frame imagery, together with satellite scenes, improves the results by taking advantage of the geometric strength of frame cameras to improve the inherent weak geometry of line cameras onboard imaging satellites. In this regard, the combination of aerial and space scenes would improve the extent of coverage as well as the geometric quality of the derived object space. The incorporation of LIDAR data, aerial images, and satellite scenes into a single triangulation procedure would also ensure the co-registration of these datasets relative to a common reference frame, which would be valuable for orthophoto generation and change detection applications.

Our future research will focus on the automation of the extraction of linear and areal features from photogrammetric and LIDAR data as well as the establishment of the correspondence between conjugate primitives. In addition, the multi-sensor triangulation environment can be used for quality assurance and quality control procedures for individual systems. For example, LIDAR-derived features can be used as a source of control for camera calibration. Alternatively, photogrammetric patches can be used for LIDAR calibration by using raw LIDAR measurements in the coplanarity constraint developed. Finally, we will investigate the development of new visualization tools for more realistic portrayal of the registration outcomes, such as texture rendering of LIDAR data, to provide a realistic view of 3D models.

## References

[1] E. Baltsavias, "A Comparison between Photogrammetry and Laser Scanning," *ISPRS Journal of Photogrammetry and Remote Sensing*, vol. 54, no. 1, 1999, pp. 83-94.

[2] D. Satale and M. Kulkarni, "LiDAR in Mapping," *Map India Conference GIS development.net,* 2003. http://www.gisdevelopment.net/technology/gis/mi03129.htm (Last accessed March 28, 2006).

[3] L. Chen, T. Teo, Y. Shao, Y. Lai, and J. Rau, "Fusion of LIDAR Data and Optical Imagery for Building Modeling," *International Archives of Photogrammetry and Remote Sensing*, vol. 35, no. B4, 2004, pp. 732-737.

[4] A. Habib and T. Schenk, "A New Approach for Matching Surfaces from Laser Scanners and Optical Sensors," *International Archives of Photogrammetry and Remote Sensing*, vol. 32, no. 3W14, 1999, pp. 55-61.

[5] M. Cramer, D. Stallmann, and N. Haala, "Direct Georeferencing Using GPS/Inertial Exterior Orientations for Photogrammetric Applications," *International Archives of Photogrammetry and Remote Sensing*, vol. 33, no. B3, 2000, pp. 198-205.

[6] H. Wegmann, C. Heipke, and K. Jacobsen, "Direct Sensor Orientation Based on GPS Network Solutions," *International Archives of Photogrammetry and Remote Sensing*, vol. 35, no. B1, 2004, pp. 153-158.

[7] T. Schenk, "Photogrammetry and Laser Altimetry," *Proc. ISPRS Workshop "Mapping Surface Structure and Topography by Airborne and Spaceborn Lasers*," vol. 32, part 3-W14, La Jolla,

California, Nov. 9-11, 1999, pp. 3-12.

[8] A. Wehr and U. Lohr, "Airborne Laser Scanning: An Introduction and Overview," *ISPRS Journal of Photogrammetry and Remote Sensing,* vol. 54, no. 2-3, 1999, pp. 68-82.

[9] H. Ebner, T. Ohlhof, and E. Putz, "Orientation of MOMS-02/D2 and MOMS-2P Imagery," *International Archives of Photogrammetry and Remote Sensing*, vol. 31, no. B3, 1996, pp. 158-164.

[10] T. Toutin, "DSM Generation and Evaluation from QuickBird Stereo Images with 3D Physical Modeling and Elevation Accuracy Evaluation," *International Journal of Remote Sensing*, vol. 25, no. 22, 2004, pp. 5181-5192.

[11] A. Habib and B. Beshah, "Multi Sensor Aerial Triangulation," *Proc. ISPRS Commission III Symposium*, Columbus, Ohio, USA, July 1998, pp. 37-41.

[12] Y. Lee and A. Habib, "Pose Estimation of Line Cameras Using Linear Features," *Proc. ISPRS Commission III Symposium "Photogrammetric Computer Vision,"* Graz, Austria, Sep. 2002.

**Sung Woong Shin** received the ME degree in civil engineering from Texas A&M University, College Station, USA, in 1998, and the PhD degree in civil engineering from the Ohio State University, Columbus, USA, in 2003. From 2003 to 2004, he was a post doctoral fellow in the Byrd Polar Research Institute at Ohio State University. Since 2004, he has been a senior member of the engineering staff in Electronics and Telecommunications Research Institute (ETRI), Daejeon, Korea. His research interests include satellite image sensor modeling, image matching, and multi-sensor data fusion.

**Ayman F. Habib** received the MSc in civil engineering from Cairo University, Egypt, the MSc and PhD in photogrammetry from the Ohio State University, USA. Currently, he is a professor with the Department of Geomatics Engineering, University of Calgary, Canada. His research interests span the fields of terrestrial and aerial mobile mapping systems, the modeling of the perspective geometry of non-traditional imaging scanners (such as line cameras), automatic matching and change detection between various datasets, automatic calibration of low cost digital cameras, the incorporation of analytical and free-form linear features in various photogrammetric orientation procedures, object recognition in imagery, and the integration of photogrammetric data with other sensors/datasets (such as GPS/INS, GIS databases, multi- and hyper-spectral sensors, and LIDAR).

**Mwafag Ghanma** received the MSc in civil engineering from Yarmouk University, Jordan, in 1987, and PhD degree from the Department of Geomatics Engineering of the University of Calgary, Canada, in 2006. Currently, he is an assistant professor with the Department of Surveying and Geomatics Engineering, Al-Balqa' Applied University, Al-Salt, Jordan. His research interests include photogrammetry, LiDAR theory and applications, geodetic and plane surveying, and digital image processing and applications.

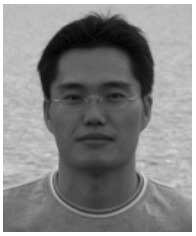

**Changjae Kim** received the BS and MS degrees in civil engineering (urban engineering major) from Seoul National University, Seoul, Korea, in 1998 and 2000, respectively. He is currently a PhD candidate at the Department of Geomatics Engineering, University of Calgary, Canada. His present research interests are virtual reality and the fusion of LIDAR with photogrammetry.

**Eui-Myoung Kim** received the MSc degree in urban engineering from Gyeongsang National University, Jinju, Korea, in 1996, and the PhD in civil engineering from Yonsei University, Seoul, Korea, in 2000. From 2000 to 2002, he was a senior researcher with Korea Institute of Construction Technology, Goyang, Korea. He worked as a post-doctoral fellow at the University of Calgary, Canada, from 2003 to 2005. He was with Korea geoSpatial Information and Communication (KSIC) in Seoul, Korea, from 2005 to 2006. Currently, he is a full-time instructor at the Department of GIS Engineering, Namseoul University, Chonan, Korea. His research interests include sensor modeling of satellite imagery, true ortho-photo generation, and GIS software development using open sources.